Assessment of the antireflection property of moth wings by three-dimensional transfer-matrix optical simulations

Olivier Deparis,[1,*] Nadia Khuzayim,[2] Andrew Parker,[2,3] and Jean Pol Vigneron[1]
[1]*Research center in Physics of Matter and Radiation (PMR), University of Namur (FUNDP), 61 rue de Bruxelles, B-5000 Namur, Belgium*
[2]*Department of Zoology, Natural History Museum, London SW7 5BD, United Kingdom*
[3]*Department of Biological Sciences, University of Sydney, New South Wales 2006, Australia*
(Received 19 December 2008; revised manuscript received 12 March 2009; published 8 April 2009)

The wings of the moth *Cacostatia ossa* (Ctenuchinae) are covered on both sides by non-close-packed nipple arrays which are known to act as broadband antireflection coatings. Experimental evaluation of the antireflection property of these biological structures is problematic because of the lack of a proper reference for reflectance measurements, i.e., a smooth surface made of the same material as the wing. Theoretical evaluation, on the other hand, is much more reliable provided that optical simulations are carried out on a realistic structural model of the wing. Based on detailed morphological characterizations, we established a three-dimensional (3D) model of the wing and used 3D transfer-matrix optical simulations in order to demonstrate the broadband antireflection property of the wings of *Cacostatia ossa*. Differences between hemispherical and specular reflectance spectra revealed that diffraction effects were not negligible for this structure although they did not jeopardize the antireflection efficiency. The influences of the backside corrugation and of the material's absorption on the reflectance spectrum were also studied. In addition, simulations based on an effective-medium model of the wing were carried out using a multilayer thin-film code. In comparison with the latter simulations, the 3D transfer-matrix simulations were found to be more accurate for evaluating the antireflection property.

DOI: 10.1103/PhysRevE.79.041910 PACS number(s): 42.66.−p, 42.70.Qs, 42.81.Qb

I. INTRODUCTION

The compound eyes of diurnal butterflies and nocturnal moths are probably the best known example of natural antireflection coatings [1]: it is also known that, 45 millions years ago, antireflection structures were already present on the eyes of a fly [2]. The antireflection layer of a compound eye consists of an array of protrusions, so-called nipples, generally dense enough not to produce diffraction: the region occupied by the nipples can be considered as a continuous layer with an effective refractive index which is the average between the corneal tissue and air, providing an intermediate refractive index appropriate for suppressing the reflection of light [3]. The height of the nipples and the distance between them are parameters that determine the antireflection efficiency optimized by millions of years of evolution of the insect group. By varying the shape of the protrusions, it is also possible to set up a gradient of effective refractive index that can favor a broadband antireflection, both spectrally and angularly. Antireflective nipple arrays were discovered by Yoshida [4] in the wings of a hawkmoth. The wings of cicadas exhibit similar nipple array corrugations and were recently used as biological templates for producing antireflection coatings [5]. Hereafter, we investigate the antireflection property of the translucent areas found on the wings of a moth, *Cacostatia ossa* (Ctenuchinae) (Fig. 1).

In the coating industry, there is a growing interest for the replication of natural antireflection nanostructures by self-assembly or templating techniques [5,6]. The experimental evaluation of the antireflection property of these bioinspired artificial coatings poses no problem since a reference—the substrate on which the coating is deposited—is readily available for reflectance measurements. For biological samples, however, such a reference is not available: for example, here, a smooth surface (at the scale of the wavelength) made of the same material as the wing does not exist. The purpose of the present theoretical study is therefore to assess the presumed antireflection property on the basis of detailed morphological characterizations of the wing. For this purpose, a three-dimensional (3D) model of the wing structure was established and 3D transfer-matrix simulations of the wing reflectance were performed. Until now, quantitative physics has not yet provided clear insight on the reverse engineering of these structures. Moreover, theoretical calculations of the reflectance of nipple array structures have been so far restricted to effective-medium approaches which can be justified to

FIG. 1. (Color online) Photograph of the moth species under study: *Cacostatia ossa* (Ctenuchinae). Scale bar: 0.5 cm. Parts of the wings appear translucent and matt, suggesting the presence of antireflection structures.

*olivier.deparis@fundp.ac.be

 ©2009 The American Physical Society

some extent by the subwavelength character of the structures but cannot intrinsically account for the light scattering by the 3D objects. Therefore, the present study will also answer questions asked by both physicists and biologists about the efficiency of these natural devices. Another point worth mentioning is that nipple array structures have often superhydrophobic property and usually perform as self-cleaning surfaces [7]. Both antireflection and superhydrophobic properties of the corneal surface provide obvious advantages for insects which rely on vision and visually mediated agility for their survival. Although only the antireflection property of *Cacostatia ossa* wings is discussed here, their plausible superhydrophobic property certainly deserves a further study.

In spite of recent advances made on the understanding of nipple array antireflection systems (see, e.g., [3] for natural systems), there are still unsolved questions. For instance, cannot we do better than effective-medium theories for modeling and interpreting the antireflection property? Is the type of periodic nipple array critical or not? How to treat disordered nipple structures? Does the presence of a symmetric corrugation on the back side (similar to *Cacostatia ossa* wing) have an influence on the antireflection? How does the material's absorption influence the reflectance? In this paper, we bring insights by addressing all these important issues.

II. MATERIALS AND METHODS

The species *Cacostatia ossa* (subfamily Ctenuchinae) belongs to Arctiidae, a large and diverse family of moths with around 11 000 species distributed worldwide. Several areas on the wings of *Cacostatia ossa* appear translucent and matt to the naked eye and might therefore possess antireflection structures (Fig. 1). The specimen we used for this study came from the collections of the Natural History Museum, London. Wing samples were cut from the specimen for detailed morphological characterizations using scanning electron microscopy (SEM) and transmission electron microscopy (TEM). The analysis of several SEM images taken from different viewing angles was found to be sufficient to extract relevant geometrical parameters of the wing model.

In theory, the quantity that characterizes the antireflection property of a photonic structure such as a nipple array is the reflectivity (or the transmittivity). This quantity, hereafter called the reflectance R_{tot}, is defined as the ratio of the electromagnetic energy flux that is scattered back into the incident medium to the incident electromagnetic energy flux. Similarly, the transmittivity, hereafter called the transmittance T_{tot}, is defined as the ratio of the flux that is scattered into the emergence medium to the incident flux. The energy conservation law implies that the absorption A, if any, is given by $A=1-R_{\mathrm{tot}}-T_{\mathrm{tot}}$.

Simulations of the reflectance (transmittance) of the wing were carried out using an original 3D transfer-matrix FORTRAN code developed at the University of Namur, Belgium [8]. The code is devoted to the calculation of the scattering properties of objects in which the dielectric permittivity ($\varepsilon=n^2$, n: complex refractive index) varies arbitrarily in the vertical direction (normal to the surface) but periodically in the lateral directions. The algorithm requires the object to be divided into layers, parallel to the surface, in which the refractive index is constant across the layer thickness. In each layer, the lateral periodic permittivity array, $\varepsilon(\mathbf{r})=\varepsilon(\mathbf{r}+\mathbf{R})$ ($\mathbf{R}$: spatial period, $\mathbf{r}=x\mathbf{e}_x+y\mathbf{e}_y$), is described by a two-dimensional (2D) plane wave expansion: $\varepsilon(\mathbf{r})=\Sigma\varepsilon_{\mathbf{g}}e^{i\mathbf{g}\cdot\mathbf{r}}$ ($\mathbf{g}$: reciprocal lattice vector). The incident wave is assumed to be a plane wave, and the incident wave vector $\mathbf{k}_{\mathrm{inc}}$ defines the incidence and azimuth angles, θ and φ, respectively. For computation purposes, each layer is further divided into slices whose thickness is much lower than the wavelength. By integrating Maxwell's equations, the electromagnetic field amplitudes at one side of a slice are expressed in terms of the amplitudes at the other side, producing the transfer matrix of the slice. For numerical stability reasons, this matrix is transformed into a scattering matrix which relates the incoming and outgoing amplitudes. Scattering matrices of all slices are assembled to give the scattering matrix of the object. The elements of this matrix are then used to calculate the field amplitudes of the scattered waves in the incidence and emergence media. These scattered waves are composed of propagating and evanescent components and emerge in all the diffraction directions associated with the reciprocal lattice vectors $\mathbf{g}$. Having determined the field amplitudes and the Poynting vectors, the corresponding energy fluxes (in the vertical direction, across the unit cell of the periodic array) are calculated. From these fluxes, the total (hemispherical) reflectance and transmittance are eventually calculated. Note that by retaining only the specular ($\mathbf{g}=\mathbf{0}$) component of the scattered waves, the specular reflectance and transmittance can also be calculated. One advantage of the Fourier representation of the fields is that the fluxes can be calculated analytically from the field amplitudes, with an accuracy that is only limited by the number of spatial frequencies used for computation. One disadvantage is the relatively long computation time. Typical CPU computation time on a single 3 GHz computing node of the ISCF supercomputer facility (Namur) was about 11 h (calculation of 401 wavelength points in the reflectance-transmittance spectrum of the photonic structure shown in Fig. 5, for a single incidence angle and a given light polarization state).

Simulations of the reflectance (transmittance) of the wing were also carried following an effective-medium approach. For this purpose, we used a multilayer thin-film FORTRAN code developed at the University of Namur and based on solving exactly Maxwell's equations for stratified media [9]. The complicated problem of the light scattering by a 3D structure was considerably simplified in this case since the problem was reduced to the calculation of the specular reflectance from a planar stratified structure.

III. MORPHOLOGICAL CHARACTERIZATION

The morphology of the wing was characterized by non-close-packed nipple arrays on both sides of the wing (Fig. 2). Assemblies of protrusions in the form of two-dimensional hexagonal arrays have often been encountered in compound eyes [3] or corrugated wings of insects [4]. As a matter of fact, in the present case, the assembly was neither highly regular nor clearly hexagonal (Fig. 3). For this reason, we

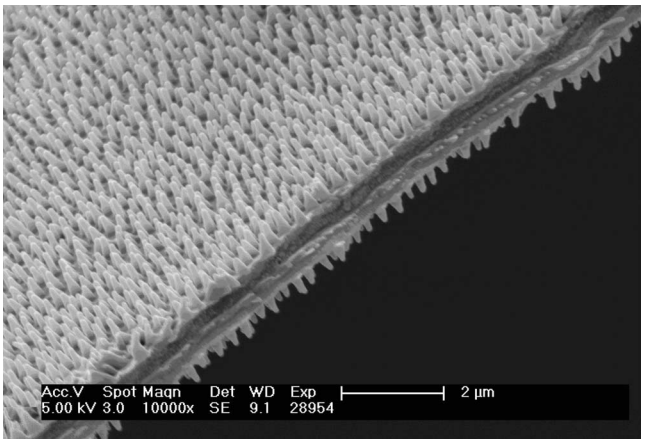

FIG. 2. SEM image of the wing of *Cacostatia ossa*: view of the wing surface at oblique incidence. Note the non-close-packed nipple arrays on both sides of the wing membrane.

chose the simplest model of a square array. Our experience in 3D transfer-matrix simulations of biological photonic structures told us that the use of a hexagonal array would not change significantly the outcomes of the present study. To check this, we performed simulations for a hexagonal array as well (see Sec. V). From the average distance between nearest neighbors, the spatial period was estimated to be $a=380$ nm. That rather long period potentially challenged the effective-medium modeling approaches. In our model of the wing (see Sec. IV), the nipples were approximated by truncated cones. The shape of the protrusions was known to affect the reflectance to a much lesser extent than their height and period (we checked this in our computations) so that the choice of truncated cone shape was not critical. From high magnification SEM images (Fig. 4), the height of the truncated cones, the radius at their base, and the radius at their top were determined to be $H=400$ nm, $R=120$ nm, and $r=50$ nm, respectively. The thickness of the bulky part of the wing was estimated to be $d=1000$ nm (Fig. 4). All dimensions given above were mean values: measured values were affected by errors due to the unavoidable disorder of the

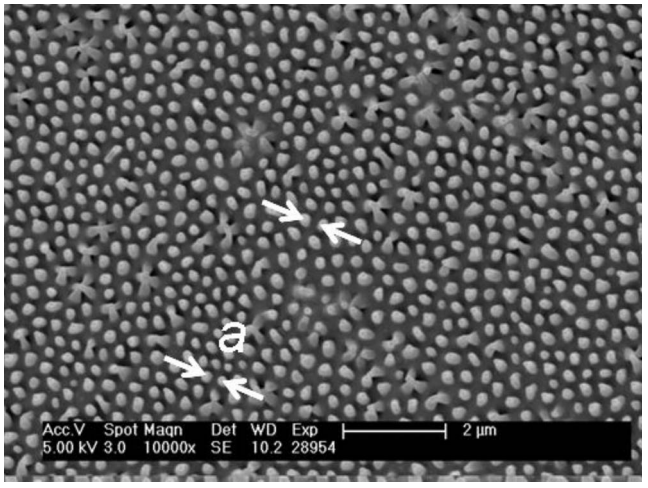

FIG. 3. SEM image of the wing of *Cacostatia ossa*: view of the wing surface at normal incidence. a: period of the nipple array.

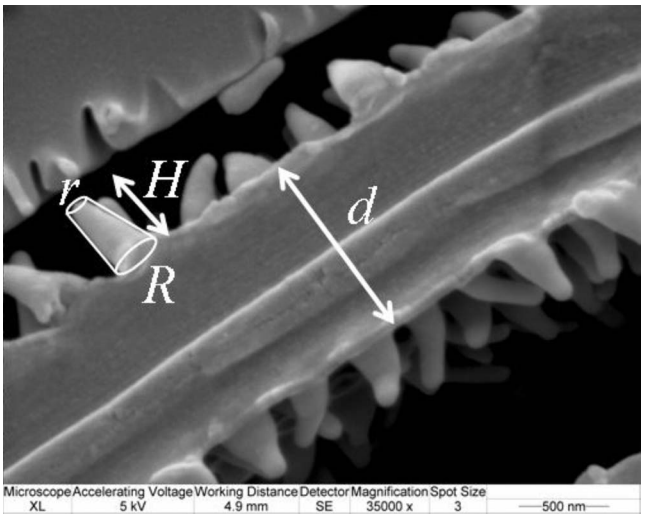

FIG. 4. SEM image of the wing of *Cacostatia ossa*: side view of a cross section of the wing. Each nipple has a truncated cone shape. R (r): radius at the cone base (top), H: truncated cone height, and d: membrane thickness.

natural structure and the reading from the SEM micrographs. Standard deviations for all reported dimensions were of the order of 5–10% and were checked not to affect the antireflection calculations significantly. In Fig. 4, the nipples appeared to be slightly crushed. This was because the sample was embedded in resin for additional measurements. Note that the original nipples appeared to be straight in Fig. 2.

IV. OPTICAL MODEL OF THE WING

On the basis of morphological data, we elaborated a 3D model of the wing which consisted of a homogeneous slab with a square array of truncated cones on both sides (Fig. 5). Both the slab and the cone arrays extended to infinity in the lateral dimensions, as required by computation codes. For the sake of simplicity, the wing was assumed to be made of a single biological material which exhibited non-negligible absorption. The complex refractive index of the material, noted as $n_c=n+ik$, was considered to be constant in the simulation spectral range in order to highlight dependencies of the reflectance on structural factors rather than on dispersion. The simulations were carried out from the near uv to the near infrared (ir), comprising the vision range of Lepidoptera (350–700 nm). Chitin was chosen as a typical constitutive material of the wing. The real part of its refractive index was taken equal to $n=1.58$ [10]. The imaginary part of the refractive index, responsible for the absorption, was taken equal to $k=0.06$, a value inspired by Ref. [11]. In order to study the influence of the wing material absorption, a lower value of k was considered ($k=0.02$). The choice of this value was guided by the achievement of transmittance values which were compatible with the translucent aspect of *Cacostatia ossa* wing (see Sec. V).

For 3D transfer-matrix numerical simulations, the wing model was divided into layers in which the refractive index was constant across the layer thickness. Therefore, a trun-

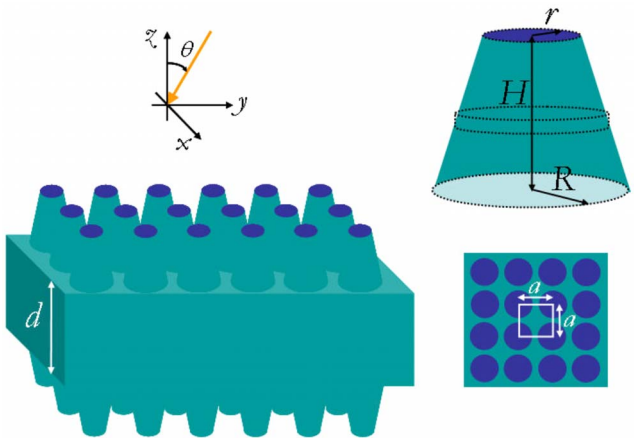

FIG. 5. (Color online) Three-dimensional model of the wing. The bulky part of the wing was modeled by a slab (thickness: d), whereas the corrugated wing surfaces were modeled by square arrays (period: a) of truncated cones. For numerical simulations, the truncated cones (height: H, radius at the base: R, and radius at the top: r) were approximated by stacks of cylinders (dotted lines). The coordinate system is shown together with the angle of incidence of the light (θ).

cated cone was approximated by a stack of cylinders of decreasing radii from the base to the top of the cone and each layer consisted of a square array of cylinders surrounded by air (n_a=1.0). The 2D spatial distribution of the refractive index was expanded into eight plane waves in both the x and y directions. The layer thickness (cylinder height) was taken equal to δ=40 nm (one tenth of the cone height H). For computation purposes, these layers (corrugated parts of the wing) were divided into 16 slices (thickness equal to 2.5 nm), whereas the homogeneous layer (bulky part of the wing) was divided into 512 slices (thickness equal to 1.95 nm). The plane of incidence was defined by the y and z axes. The incident light was linearly polarized either transverse electric (TE), i.e., electric field aligned along the x axis, or transverse magnetic (TM), i.e., electric field lying in the yz plane. Both normal and tilted incidence conditions were considered. Either the specular or the total (hemispherical) reflectance and transmittance was calculated for wavelengths ranging from the near-uv to the near infrared regions.

For comparison, an effective-medium model of the wing was also elaborated. In this approach, the 2D-structured layers were replaced by homogeneous layers of effective refractive index n_e (complex number). Considering that the unit cell of the 2D-structured layers had a square cross section and consisted of a circular cylinder embedded in air, the material's volume filling factor in the jth layer was given by $f_j=\pi(r_j/a)^2$, where r_j was the cylinder radius in the jth layer (r_j varied between R and r according to the altitude z). Previously reported modeling studies on nipple arrays used the following approximated mixing formula for calculating the effective index [3]:

$$n_{e,j}=[f_j n_c^q+(1-f_j)n_a^q]^{1/q}, \tag{1}$$

where q=2/3. For a fair comparison with the 3D transfer-matrix simulations, we used the same formula and took the effective-medium layer thickness equal to the 2D-structured layer thickness (δ=40 nm). We also checked that decreasing further the layer thickness (δ=10 nm) had negligible effect on the calculated reflectance.

In the model, we considered that the wing membrane was homogenous. Actually, by careful inspection of high magnification SEM cross-section images (not shown here), we found evidences of a periodic stack of about 15 layers embedded within the membrane. The layer thicknesses, however, were too small to produce a Bragg reflectance peak in the wavelength range above 250 nm even when considering the highest possible refractive index contrast (chitin/air). According to simple multilayer film calculations, the Bragg peak was found to be located around 120 nm. Clearly, this embedded multilayer structure could not affect the visual aspect of the wing and could therefore be omitted from our 3D model.

V. SIMULATION RESULTS

In most of the results presented hereafter, we selected those relative to the TE polarization state of the incident light in order to focus on other factors influencing the antireflection property. Similar conclusions could be drawn for the TM polarization state which was also used in our calculations. The reflectance spectrum was first calculated for the bare wing (i.e., with a smooth surface at the nanolevel, modeled by a slab of thickness d) at normal incidence using the multilayer thin-film code. This calculation served as a reference for the evaluation of the antireflection property of the corrugated wing. The reflectance spectrum of the bare wing exhibited typical oscillations due to thin-film interference around an average level of about 5% (Fig. 6, dashed line). The total reflectance spectra of corrugated wings were then calculated at normal incidence using the 3D transfer-matrix code. Two wing models were considered: a wing model with square nipple array corrugations on both sides (Fig. 5) and a wing model with corrugation only on the side facing the incidence medium. The former model represented the natural configuration of the wing, whereas the latter was devised to examine the influence of the backside corrugation. The calculated reflectance spectrum of the double-sided corrugated wing model (Fig. 6, thin solid line) demonstrated the broadband antireflection property of the real wing: within the insect vision range (350–700 nm), on average, the reflectance is reduced by 1 order of magnitude. In the absence of the corrugation on the backside, the antireflection effect was found to be slightly less efficient (Fig. 6, thick solid line). This influence was due to the fact that the backside surface gave some contribution to the amount of light that was reflected in the incidence hemisphere: a corrugated backside surface helped to increase light transmission from the bulk of the wing to the air and therefore to reduce the wing reflectance on overall. The reflectance spectra of effective-medium wing models were also calculated at normal incidence using the multilayer thin-film code (Fig. 6, square and circle dotted lines). These calculations gave spectra that were different from the previous ones: the antireflection effect, averaged on the uv-visible range, turned out to be slightly underesti-

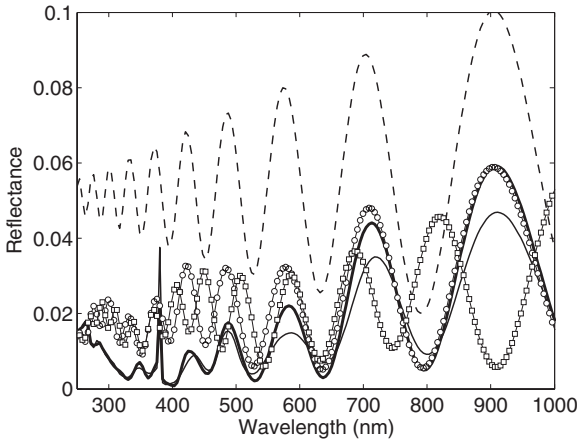

FIG. 6. Reflectance spectra calculated for different wing models at normal incidence: bare wing (dashed line), wing with square nipple arrays on both sides (thin solid line and square dotted line), wing with a square nipple array on the incidence side only (thick solid line and circle dotted line). Total (hemispherical) reflectance was calculated using a 3D transfer-matrix code applied to the 3D structure of the wing (solid lines). Specular reflectance was calculated using a multilayer thin-film code applied to a slab (dashed line) or to an effective-medium approximation of the wing structure (square or circle dotted lines). The wing refractive index was taken equal to $n_c = 1.58 + i0.06$.

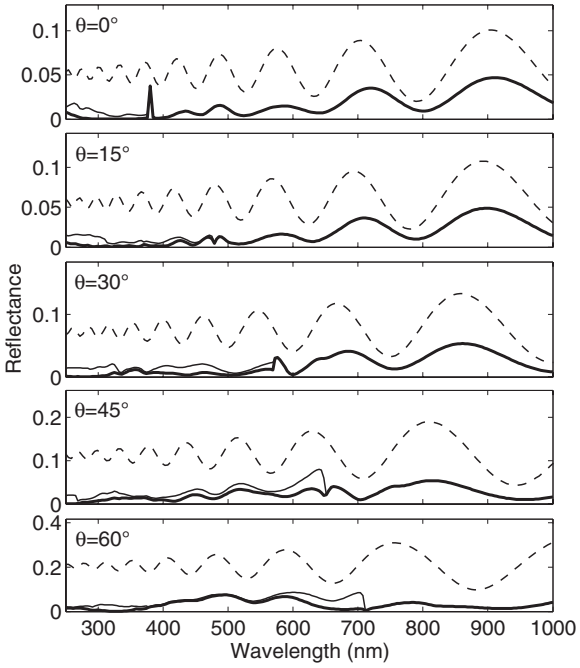

FIG. 7. Reflectance spectra calculated for the double-sided corrugated wing model at various angles of incidence (TE polarized light) using a 3D transfer-matrix code: total (hemispherical) reflectance (thin solid lines) and specular reflectance (thick solid lines). Specular reflectance of the bare wing (dashed lines) was calculated using a multilayer thin-film code. The wing refractive index was taken equal to $n_c = 1.58 + i0.06$.

mated. These differences were due to the fact that the effective-medium models were intrinsically not able to account for the 3D character of the wing structure. An evidence for this was the peak around the wavelength corresponding to the periodicity of the corrugation (380 nm) which was observed in the 3D transfer-matrix simulations but not in the effective-medium simulations. This peak arose from diffraction of the 3D wing structure, as discussed hereafter.

Total and specular reflectance spectra were calculated for the double-sided corrugated wing model at various angles of incidence using the 3D transfer-matrix code (Fig. 7). As expected for nipple array corrugated structures, the antireflection effect was also found to be angularly broadband. In a certain wavelength range, depending on the angle of incidence, the total reflectance was higher than the specular reflectance due to diffraction. The diffraction of the light by the 3D wing structure was fully accounted for by our 3D transfer-matrix code. However, in order to gain an intuitive insight into such a complex situation, we performed a simple estimation on the basis of the diffraction law applied to a one-dimensional grating. First, we used the formula

$$\sin \phi = \sin \theta \pm m\frac{\lambda}{a} \tag{2}$$

to calculate the angle ϕ at which light could be diffracted into the mth order: taking $a = 380$ nm, the formula predicted that, at $\lambda = 500$ nm, no diffraction could take place for $\theta = 0°$ or $\theta = 15°$, in agreement with the simulations where both the total and specular reflectance values were equal at that wavelength (Fig. 7). However, first-order diffraction ($m = -1$) was predicted for $\theta = 30°$ at the same wavelength, in agreement with the simulations where a difference between total and specular reflectance values was observed (Fig. 7). In this case, the diffraction angle was calculated to be $\phi = -54.7°$. The wavelength at which the first (negative) order of diffraction appeared for a given angle of incidence was then determined by setting $\phi = -90°$ in the formula. At $\theta = 30°$, for example, we found $\lambda = 570$ nm in perfect agreement with the simulation (Fig. 7). The diffraction formula also predicted that the onset of diffraction shifted to longer wavelengths as the angle of incidence was increased, as observed in the simulations. The 3D transfer-matrix simulations therefore revealed that diffraction had an influence on the reflectance of *Cacostatia ossa* moth wing in the uv-visible range but this effect was not strong enough to jeopardize the antireflection property.

The current knowledge on nipple arrays tells us that the protrusions have to be more or less densely packed in order to produce a significant antireflection effect. In case of a periodic array of protrusions, the period should therefore not be too large in comparison with the protrusion width. In our case (see Fig. 5), it implies that $a/(2R) \simeq 1$ (with the condition $a \geq 2R$ so that nearest protrusions do not overlap). In the reported simulations, $a/(2R) = 380/240 = 1.6$, meaning that the packing density of the nipple array is significantly lower than in the close-packed situation $[a/(2R) = 1]$. In spite of this relatively low packing density, the structure performs well in terms of antireflection. This result confirms that the period is not a critical parameter provided that it is reasonably short to form a more or less dense array. Such a behavior contrasts with, for instance, the iridescence of 3D photo-

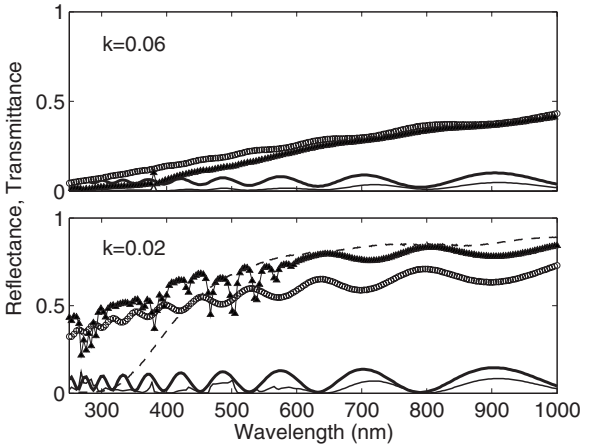

FIG. 8. Reflectance spectra (solid lines) and transmittance spectra (circle and triangle dotted lines) of the bare wing (thick solid line and circle dotted line) and of the double-sided corrugated wing (thin solid line and triangle dotted lines) calculated at normal incidence for two different values of the wing's absorption: $k=0.06$ (top chart) and $k=0.02$ (bottom chart). Total (hemispherical) reflectance and transmittance of the double-sided corrugated wing was calculated using a 3D transfer-matrix code. Specular reflectance of the bare wing was calculated using a multilayer thin-film code. The transmittance of *Cacostatia ossa* wing was also measured at normal incidence (dashed line).

nic crystals, where the property of interest (narrow-band reflectance peak) is highly sensitive to the periodicity of scatterers.

The influence of the material absorption on the reflectance and transmittance of the wing was studied. Simulations of the reflectance and transmittance of the bare wing and of the double-sided corrugated wing were carried out at normal incidence for $k=0.06$ and 0.02 (Fig. 8). As the absorption coefficient was decreased by a factor of 3 (0.02 instead of 0.06), the thin-film oscillations in the bare wing model became larger (when the membrane is less absorbing, a larger number of internal reflexions can contribute to the interference) but the antireflection effect in the double-sided corrugated wing model persisted, although being slightly less pronounced on average. The decrease in the absorption coefficient led to an enhanced transmittance. The spectral transmittance of *Cacostatia ossa* wing was measured at normal incidence using a CARY 500 uv-vis-near-ir spectrophotometer. The measured transmittance values in the visible range confirmed the translucent aspect of the wing and suggested that the actual value of k was likely to be closer to 0.02 than to 0.06 (discrepancies in the uv region were likely due to the dispersion of the chitin absorption). The value of $k=0.06$ can therefore be considered as a worst case. The good agreement between measured and simulated transmittance spectra showed the ability of the 3D model to describe the wing of *Cacostatia ossa*.

Finally, square and hexagonal array models were compared on the basis of the total reflectance spectra calculated for both TE and TM polarized light at oblique incidence (Fig. 9). For a fair comparison, the same value was taken for the square side and the hexagon side, which corresponded to the average distance between nearest protrusions (380 nm). The

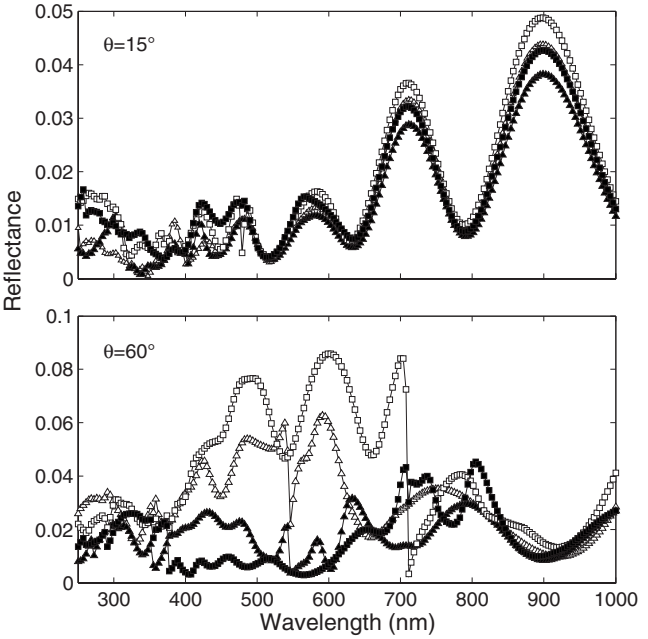

FIG. 9. Reflectance spectra calculated for a square array model (square dotted lines) and a hexagonal array model (triangle dotted lines) of the double-sided corrugated wing, at 15° (top) and 60° (bottom) incidence, for TE (open squares or triangles) and TM (filled squares or triangles) polarized light. Total (hemispherical) reflectance was calculated using a 3D transfer-matrix code. The square side and the hexagon side were taken equal to 380 nm. The wing refractive index was taken equal to $n_c=1.58+i0.06$.

two wing models gave very similar reflectance spectra for both polarizations. This result justifies our choice of a simple square array for representing the actual wing corrugation. Regarding the relatively disordered aspect of the protrusion assembly, we note that a standard technique for treating disordered structures would consist in averaging reflectance spectra calculated for a large number of periodic structures having dimensions consistent with the average distance between scatterers. The high degree of similarity found here between the reflectance spectra of two different periodic models indicates the robustness of the reflectance and therefore of the antireflection property, with respect to disorder. In the case of *Cacostatia ossa* wing, the partial disorder in the actual structure is likely to reduce the already small diffractive effects but not to compromise the predicted antireflection property.

VI. CONCLUSIONS

Three-dimensional transfer-matrix simulations of the reflectance of translucent moth wings were performed in order to assess the antireflection property of the wings. The wing model was elaborated on the basis of detailed morphological characterizations of wing samples at the nanometer scale. Non-close-packed, more or less periodic arrangements of nipplelike protrusions were found on both sides of the wings and modeled by two-dimensional periodic square arrays of truncated cones. The simulations indicated the spectrally and angularly broadband antireflection of the wing structure and

a non-negligible contribution from diffraction. Similar results were obtained with a hexagonal array model, showing the robustness of the antireflection property with respect to disorder. The investigated antireflection structure was found to be particularly efficient in, and therefore adapted to, the near-uv/visible range. The simulated reflectance spectra were more accurate than those obtained by effective-medium theory, and therefore, we believe they will be helpful to scientists and engineers who currently develop bioinspired antireflection coatings. Although the model of any natural structure can always be improved, we believe that our double-sided square array model is, to a very reasonable extent, a representative of the actual wing structure of *Cacostatia ossa*. In the coating industry, the fabrication processes are expected to set tight tolerances on the structure dimensions and periodicity. Therefore, in this context, more accurate models should be readily available and the theoretical approach presented here for periodic structures is highly promising.

ACKNOWLEDGMENTS

This investigation was conducted with the support of the European NEST STREP BioPhot project (Contract No. 12915) and the Australian Research Council (grant to ARP). The authors acknowledge the use of Namur Interuniversity Scientific Computing Facility "Namur-iSCF," a common project between the Belgian National Fund for Scientific Research (FNRS) and the University of Namur (FUNDP), Belgium.

[1] W. H. Miller, A. R. Moller, and C. G. Bernhard, *The Functional Organization of the Compound Eye* (Pergamon, Oxford, 1966).
[2] A. R. Parker, Z. Hegedus, and R. A. Watts, Proc. R. Soc. London, Ser. B **265**, 811 (1998).
[3] D. G. Stavenga, S. Foletti, G. Palasantzas, and K. Arikawa, Proc. R. Soc. London, Ser. B **273**, 661 (2006).
[4] A. Yoshida, Forma **17**, 75 (2002).
[5] G. Xie, G. Zhang, F. Lin, J. Zhang, Z. Liu, and S. Mu, Nanotechnology **19**, 095605 (2008).
[6] A. R. Parker and H. E. Townley, Nat. Nanotechnol. **2**, 347 (2007).
[7] T. Wagner, C. Neinhuis, and W. Barthlott, Acta Zoologica **77**, 213 (1996).
[8] J. P. Vigneron and V. Lousse, Proc. SPIE **6128**, 61281G (2006).
[9] A. Dereux, J. P. Vigneron, P. Lambin, and A. A. Lucas, Phys. Rev. B **38**, 5438 (1988).
[10] M. F. Land, J. Horwood, M. L. M. Lim, and D. Li, Proc. R. Soc. London, Ser. B **274**, 1583 (2007).
[11] P. Vukusic, J. R. Sambles, C. R. Lawrence, and R. J. Wootton, Proc. R. Soc. London, Ser. B **266**, 1403 (1999).